On the different faces of the supercritical phase of water at a near-critical temperature: Pressure-induced structural transitions ranging from a gas-like fluid to a plastic crystal polymorph.

Ioannis Skarmoutsos [a,*], Andrés Henao[b], Elvira Guardia [c] and Jannis Samios [d]

[a] *Theoretical and Physical Chemistry Institute, National Hellenic Research Foundation, Vas. Constantinou 48, GR-116 35, Athens, Greece*
[b] *Dynamics of Condensed Matter and Center for Sustainable Systems Design, Department of Chemistry, University of Paderborn, Warburger Str. 100, D-33098 Paderborn, Germany.*

[c] *Departament de Física, Universitat Politècnica de Catalunya, Campus Nord-Edifici B4-B5, Jordi Girona 1-3, Barcelona E-08034, Spain.*

[d] *Department of Chemistry, Laboratory of Physical Chemistry, National and Kapodistrian University of Athens, Panepistimiopolis 157-71, Athens, Greece*

Abstract

The present study reports a systematic analysis of a wide variety of structural, thermodynamic and dynamic properties of supercritical water along the near-critical isotherm of T=1.03 T_c and up to extreme pressures, using molecular dynamics and Monte Carlo simulations. The methodology employed provides solid evidence about the existence of a structural transition from a liquid-like fluid to a compressed, tightly-packed liquid, in the density and pressure region around 3.4 ρ_c and 1.17 GPa, introducing an alternative approach to locate the crossing of the Frenkel line. Around 8.5 GPa another transition to a face-centered cubic plastic crystal polymorph with density 5.178 ρ_c is also observed, further confirmed by Gibbs free energy calculations using the two-phase thermodynamic model. The isobaric heat capacity maximum, closely related to the crossing of the Widom line, has also been observed around 0.8 ρ_c, where the local density augmentation is also maximized. Another structural transition has been observed at 0.2 ρ_c, related to the transformation of the fluid to a dilute gas at lower densities. These findings indicate that a near-critical isotherm can be divided in different domains where supercritical water exhibits distinct behavior, ranging from a gas-like to a plastic crystal one.

[*] email: iskarmou@eie.gr

1. Introduction

According to the standard physical chemistry textbooks the liquid and gas phases of a molecular system can coexist under specific (P,V,T) conditions up to the critical point (P_c, V_c, T_c), where a stationary inflection point on the P-V critical isotherm is observed[1]. The isothermal compressibility factor of the system also diverges as the critical point is approached[2]. According to keynote reviews[3], the actual definition of a supercritical fluid (SCF) is that of a fluid at a temperature higher than its critical value T_c, regardless of its pressure and density. Up to about a decade ago, the generally accepted idea was that there isn't any physical observable capable to distinguish the liquid and gas phases of a molecular system at supercritical conditions[4]. However, experimental and theoretical studies revealed the existence of maxima for some thermodynamic properties, such as the specific heat, the thermal expansion coefficient and the isothermal compressibility[4-12]. The location of these maxima defines a line arising from the critical point, which has been characterized as the Widom line[4-12]. Although not related to any first- or second-order transition, this line is considered as the boundary of two different dynamical regimes, a gas- and a liquid-like one.

The structure and dynamics of near-critical SCFs exhibit another peculiar behavior. Their microscopic picture resembles that of an inhomogeneous system with voids and molecular clusters exhibiting a local density augmentation[3]. Our previous systematic studies have shown that these local density augmentation effects and corresponding local density relaxation times depend strongly on the nature of the intermolecular interactions and are maximized in the density region around 0.8 ρ_c[13-15]. At densities higher than 2.0 ρ_c the formation of voids is no longer pronounced. At higher pressures SCFs exhibit a crossover in several properties, often characterized by the introduction of a new line called the Frenkel line[16-25], which is still a subject of debate [23-25] and an active area of research in order to achieve a deep understanding of the molecular-scale phenomena taking place at high pressures.

Among several SCFs, supercritical water (SCW) is of paramount importance for a wide range of applications in physics, chemistry, materials and earth science[26-28]. The complex behavior of water is reflected on its phase diagram, with very distinct liquid and solid

phases observed so far at very different thermodynamic conditions[29]. At high temperatures and extreme pressures evidences of the existence of plastic crystal phases of water range have also been reported in classical and ab initio molecular simulation studies[29-37]. However, the detailed analysis of the structure and dynamics of these plastic crystal phases, as well as the transformation boundaries and mechanisms between the so-far computationally reported polymorphs, at supercritical conditions is still an open topic of investigation. In this respect, molecular simulation can be an extremely useful tool in predicting the behavior of SCFs at extreme conditions, and can further guide and assist the design of experiments[38].

Here, by applying molecular simulation techniques, we initially focused on the behavior of SCW at the high-pressure regime, along a near-critical isotherm ($T=1.03\ T_c$), aiming to shed some light on the existence or not of structural transitions at densities higher than 2.0 ρ_c, by systematically investigating the density dependence of a wide variety of structural, thermodynamic and dynamic property descriptors.

As mentioned above, the maximum in thermodynamic quantities such as the isobaric heat capacity C_p at densities lower than 2.0 ρ_c is attributed in the literature to structural transitions from a gas-like to a liquid-like inhomogeneous fluid. The temperature dependence of the thermodynamic state points related to these structural transitions is represented by the introduction of the Widom line. In a previous study[39] we had performed a structural analysis based upon the identification of nearest neighbors and the estimation of the volume of the sphere containing the four nearest neighbors around a central water molecule. Our analysis had revealed a very sharp increase of this volume at densities lower than 0.2 ρ_c. The observation of this crossover provided an indication that in this range of densities the short-range order is destroyed and a structural transition takes place in the system. However, it was not yet clarified if this structural crossover is related to the structural transitions described by the Widom line or not. Therefore, another aim of the present study was to locate the maximum in the C_p along the investigated near-critical isotherm in order to see if the above-mentioned structural crossover at 0.2 ρ_c is related to the Widom line or not.

In general, the present study aims to provide a systematic analysis of the thermodynamic, structural and dynamic features of the fluid in a very wide pressure range along a near-critical isotherm, presenting a unified picture of the several different structural regimes of SCW and the corresponding structural transitions at near-critical conditions, ranging from a gas-like fluid to a plastic crystal polymorph.

The manuscript has been organized in the following way: In Section II the employed computational methods are presented, whereas the results and the relevant discussion are presented in Section III. Finally, the concluding remarks are provided in Section IV.

2. Computational Methods

2.1 Fluid-phase simulations

Classical NVT Monte Carlo (MC) and NVT molecular dynamics (MD) simulations of SCW were initially performed in the density range 2.2-4.6 ρ_c along the near-critical isotherm of T=1.03 T_c (T_c = 647.1 K, ρ_c = 0.322 g/cm^3), using the SPC/E[40] potential model of water. To explore additional thermodynamic state points when investigating the density-pressure diagram of SCW at higher pressures close to the melting line, another NVT MC and NVT MD simulation at the density of 4.8 ρ_c was afterwards performed. Apart from the simulations in the density range 2.2-4.8 ρ_c, additional NVT MC simulations were performed in the range 0.05-2.0 ρ_c. Subsequently, NPT MC simulations were performed at fixed pressures corresponding to the ones calculated from all the NVT MC runs, to investigate the pressure and density dependence of the specific heat of SCW. The choice of the SPC/E model has been based upon previous works verifying its accuracy in estimating the critical point of water as well as various thermodynamic, structural, transport and dynamic properties of the system[39, 41-45]. Moreover, the use of SPC/E potential model allowed us to correlate our findings with results previously obtained at the density range 0.05-2.0 ρ_c using the same model[39]. Note that the simulated fixed densities have been expressed as reduced densities ρ/ρ_c, using as reference the experimental critical density. The reason to do so is that the reported values for the calculated critical density using the SPC/E model are close to the experimental one. Furthermore, since the value of the calculated critical density may slightly depend on the simulation method[41,42,46], it was considered as a more standard approach to use the experimental critical density as a

reference point. In this way the findings of the present study could be also correlated to the findings of our previous works[13-15,39], providing in this way a more complete picture of the behavior of SCW at supercritical conditions near the critical point. The temperature of the selected isotherm is also higher than the predicted critical temperature of SPC/E water, ensuring that the simulated fluid water is a supercritical fluid. MC simulations in the canonical ensemble have been performed using 500 water molecules in cubic boxes for 500000 MC cycles using the RASPA code[47] to equilibrate the systems under study. The equilibrated configurations were used as starting points for subsequent 5 ns MD equilibration runs using the DL_POLY code[48], followed by 10 ns production runs to calculate the properties of the systems. A 9 Å cutoff was used in the simulations to treat the van der Waals interactions, while the long-range electrostatic interactions were treated using the standard Ewald summation method[49]. The equations of motion in the MD simulations were integrated using a leapfrog-type Verlet algorithm[49] and the integration time step was set to 1 fs. The intramolecular geometry of the water molecules was constrained using the shake algorithm[49] and the pressure and temperature were constrained using Nose-Hoover thermostats[50] and barostats[51].

Trial runs with 864 and 1372 molecules confirmed the absence of system-size effects on the obtained results. The calculated pressures corresponding to each one of the simulated densities were used as inputs in subsequent NPT MC simulations to calculate the constant-pressure heat capacity of SCW.

2.2 Investigation of the stability of the face-centered cubic plastic crystal phase

Additional NPT MD simulations at higher pressures were performed in order to investigate the face-centered cubic (fcc) plastic crystal phase of water. Following previously established simulation protocols, initial fcc configurations containing 500 water molecules with random orientations in a cubic box were prepared. Previous studies[29,37] have reported that the fcc plastic crystal phase stabilized by this protocol perfectly reproduces the fcc plastic crystal obtained during the Martensitic phase transition of the bcc plastic crystal phase, using anisotropic NPT-MD simulations techniques. The system was then equilibrated for 100 ns in the NPT-ensemble for a series of pressures in the range P=8.5-11 GPa and T=1.03 Tc. The simulations revealed that at pressures higher than 8.5 GPa after

100 ns the plastic crystal structure was maintained, while at pressures lower than 8.5 GPa trial runs revealed that the initial fcc crystal structure melts fast and transforms to a high-pressure liquid-like fluid. The calculated density for the fcc plastic crystal phase at 8.5 GPa was found to be 5.178 ρ_c (1.667 g/cm^3). To further investigate the thermodynamic stability of the fcc plastic crystal phase, two NPT-MD simulations at 8.5 GPa were performed, starting from a random, fluid-like, initial configuration. The first isotropic NPT-MD simulation with 432 water molecules was performed to see if the system at 8.5 GPa converts to a bcc plastic crystal phase. This methodology according to the literature and our previous works at subcritical temperatures[29,30,31,36,37] is very effective in reproducing this plastic crystal phase at temperature and pressure conditions where the fluid- plastic bcc transition is thermodynamically favorable. Our simulation has shown that the system does not convert to a plastic bcc crystal after 100 ns of simulation at these thermodynamic conditions (1.03 T_c, 8.5 GPa). An additional isotropic NPT-MD run was performed at the same conditions using an initial configuration of a plastic bcc crystal of 432 water molecules in a cubic box, obtained at T=440 K and 9 GPa, using the same computational protocol as in our previous studies[36,51]. In this case it was observed that even if we start from an initial plastic bcc crystal structure, the system converts to a fluid phase after a few ps. In both cases the density of the fluid phase at T=1.03 T_c and 8.5 GPa converges to the same value of 4.976 ρ_c (1.602 g/cm^3) independently of the initial configuration. These findings are in agreement with previous studies[33] mentioning that at high temperatures the bcc plastic crystal phase is observed at higher pressures in comparison with the fcc one, which is more stable at the investigated pressure range. To further compare the stability of the fcc plastic crystal phase, a 100 ns NPT-MD simulation was performed with 500 molecules staring again from a random fluid-like initial configuration. The resulting phase after 100 ns is a liquid-like fluid phase. The density of the obtained liquid-like phase is the same with the one obtained when using 432 molecules in the simulation box. Next, two NVT-MD simulations were performed at the calculated densities of the predicted fcc plastic crystal phase and liquid-like fluid phase at 8.5 GPa. The two systems were again equilibrated for 5 ns and additional production runs of 10 ns were then employed to determine structural and dynamic properties. Using the trajectories of these simulations, we applied the two-phase thermodynamic model[52,53], as implemented in the DoSPT code[54],

in order to estimate the entropy of the two phases. In the framework of the two-phase thermodynamic model[52,53] a fluidicity parameter, corresponding to the thermodynamic conditions of the simulated system, is used to partition the translation and rotation modes into a diffusive, gas-like component and a non-diffusive, solid-like component. The entropy of a molecular system is obtained by calculating the density of state functions from the Fourier transform of the corresponding velocity autocorrelation functions and subsequently applying quantum statistics to the solid component and hard sphere/rigid rotor thermodynamics to the gas component. A detailed description of the two-phase thermodynamic model is provided in the literature[52-54]. By calculating the entropy S of the simulated fcc plastic crystal and liquid-like fluid phases, the Gibbs free energy of each phase was calculated from the trajectories of the NVT-MD simulations using the standard thermodynamic formalism:

$$G = \left\langle E^{tot} \right\rangle - T \cdot \left\langle S \right\rangle + \left\langle P \right\rangle \cdot V = \left\langle U^{pot} + E^{kin} \right\rangle - T \cdot \left\langle S \right\rangle + \left\langle P \right\rangle \cdot V \quad (1)$$

In this equation $\left\langle U^{pot} \right\rangle$ and $\left\langle E^{kin} \right\rangle$ are the average potential and kinetic energy calculated by the NVT-MD simulations of the two phases. Using this formalism, the estimated Gibbs free energy values for the fcc plastic crystal and the liquid-like fluid phase are 17.19 and 24.18 kJ/mol, respectively. The fact that the corresponding Gibbs free energy change for the fluid→ plastic fcc crystal transition is $\Delta G = -6.99$ kJ/mol clearly indicates that the fcc plastic crystal phase is the most thermodynamically stable phase, further verifying the existence of this transition. Therefore, our simulations indicate that at T=1.03 T_c and 8.5 GPa SCW is crossing a melting line converting to a fcc plastic crystal polymorph. Characteristic snapshots of the simulated metastable, liquid-like phase and the fcc plastic crystal phase of water are depicted in Figure 1. Selective snapshots from the simulations performed in the present work, starting from low densities (0.2 ρ_c) and going up to the observed fcc plastic crystal phase at 8.5 GPa (with a density of 5.178 ρ_c) are also presented in Figure 2, clearly depicting the structural changes as the density of the system increases.

3. Results and Discussion

3.1. Local Intermolecular Structure – Hydrogen Bonding

To explore the structural changes in SCW at the density region 2.2 - 4.6 ρ_c, along the isotherm T=1.03 T_c, the calculated, and presented in Figure 3, O-O and O-H pair radial distribution functions (rdf) were analyzed in detail. To further validate the efficiency of the SPC/E potential model in predicting the structure of SCW at high densities and pressures, an additional NVT-MD simulation was performed at a slightly higher temperature T= 1.04 T_c (673 K) and a density of 2.71 ρ_c where Soper, using an empirical potential structure refinement of his experimental neutron diffraction (ND) data[55], presented these rdfs. The calculated rdfs in our present study are in good agreement with the experimental ones, as it can be seen in Figure 4. The only difference between the calculated rdfs and the ones obtained by Soper is the slightly higher intensity of the first peak of the O-H rdf obtained by the MD simulations with the SPC/E potential model. As the density increases, SCW starts to resemble a dense liquid, with the appearance of well-defined first, second and third solvation shells at short intermolecular distances. The positions of the minima are also slightly shifted to shorter distances at higher densities. This behavior is also reflected on the much larger first shell's coordination number, with its corresponding values ranging from 7.3 to 14.2 in the density range 2.2 - 4.6 ρ_c.

The changes in the behavior of SCW at densities higher than 2.0 ρ_c are also reflected on the density dependence of the average number of hydrogen bonds (HBs) $<n_{HB}>$ formed per molecule, presented in Figure 5. To estimate these numbers, a well-established geometric criterion, used in several previous studies[13,39,56-58], was employed. According to this criterion a hydrogen bond between two water molecules exists if the interatomic distances are such that R(O…O) $\leq$ 3.6 Å, R(H…O) $\leq$ 2.4 Å and the donor-acceptor angle H-O…O $\leq$ 30º (the symbol ... corresponds to intermolecular distances). It can be clearly observed that in the density range 2.2 - 4.6 ρ_c $<n_{HB}>$ exhibits a linear density dependence. By analyzing in the present study the trajectories of our previous MD simulations[38] in the density range 0.2 - 2.0 ρ_c, it was found that $<n_{HB}>$, presented in the inset picture in Figure 5, exhibits a non-linear density dependence due to the local density augmentation effects in this particular region. The change in the density dependence of $<n_{HB}>$ at densities higher

than 2.0 ρ_c is a further indication of the liquid-like behavior of SCW at higher densities. The density dependence of the fractions f_n of water molecules forming n HBs (n=0-5), presented in Figure 5, also provides interesting information about the local structural changes in SCW in the density range 2.2 - 4.6 ρ_c. At 2.2 ρ_c the dominating fractions of hydrogen bonded water molecules are f_2 and f_1. However, at 3.4 ρ_c the fraction of molecules forming 3 HBs starts being the dominating one and several intersections between different $f_n(\rho)$ curves are observed. At this particular density $f_2 \approx f_3$, $f_1 \approx f_4$ and $f_0 \approx f_5$, respectively. At 4.6 ρ_c the dominating fractions of hydrogen bonded molecules are f_3 and f_4. Note however that, although at high densities the coordination number for the first solvation shell of water is quite large (14.2 at 4.6 ρ_c) the average number of HBs per molecule is still lower in comparison with ambient water, indicating a loss of local orientational order at the tightly packed first solvation shell of SCW at high densities.

The density effects on the local orientational order in high-density SCW were studied by calculating the commonly used tetrahedral[59] q and trigonal order q_3 parameters[60] and the entropic parameter S_q, related to the tetrahedral entropy per molecule [61], which are presented in Figure 6. The tetrahedral order parameter[59] gives information about the tetrahedral arrangement of the four nearest neighbors of each water molecule and is defined as:

$$q = 1 - \left\langle \frac{3}{8} \sum_{j=1}^{3} \sum_{k=j+1}^{4} \left(\cos\varphi_{jik} + \frac{1}{3} \right)^2 \right\rangle \qquad (2)$$

where ϕ_{jik} corresponds to the angle formed by the vectors $\vec{r}_{ij}$ and $\vec{r}_{ik}$, connecting the oxygen atom of the central molecule i with the oxygen atoms of two of its four nearest neighbors j, k. The trigonal order parameter[60] q_3 is defined, taking into account the three closest neighbors of a given molecule i, as:

$$q_3 = 1 - \left\langle \frac{4}{7} \sum_{j=1}^{2} \sum_{k=j+1}^{3} \left(\cos\phi_{jik} + \frac{1}{2} \right)^2 \right\rangle \qquad (3)$$

These order parameters have been normalized to one for perfect order and zero for a random distribution. The entropic term S_q is associated with the local tetrahedral order

around the water molecules and can be calculated from the probability distribution of the tetrahedral order parameter f(q):

$$S_q = \frac{3}{2}\cdot\frac{1}{N}k_B\sum_{i=1}^{N}\ln\left(1-q_i\right) = \frac{3}{2}\cdot k_B\int \ln\ \left(1-q\right)\cdot f(q)\cdot dq \qquad (4)$$

In Eq. 4, k_B is the Boltzmann constant. As it can be observed, around 3.4 ρ_c q and q_3 are maximized, whereas S_q minimized. The appearance of these local extrema in this particular region could be related to structural transitions from a liquid-like fluid to a tightly packed liquid, where a loss of the local orientational ordering is observed due to the very dense packing of the molecules at short intermolecular distances. The position of these extrema could therefore be used to identify the boundary for the structural transitions from a "non-rigid" to a "rigid" liquid, with the latter being dominated by the very strong repulsive interactions between the molecules which are tightly packed at short intermolecular distances. Note that our previous studies[39] in the density region 0.2-2.0 ρ_c revealed that the q and q_3 exhibit a non-linear density dependence very similar to the one observed for the average number of HBs per molecule, which has been attributed to the local density inhomogeneities in this particular region. All the above results sufficiently indicate that the structure of SCW in the density regions 0.2-2.0 ρ_c, 2.2 -3.4 ρ_c and 3.4-4.6 ρ_c is significantly different, as also depicted in the snapshots of the simulations presented in Figure 2.

To further investigate the density dependence of the local translational order in SCW, we calculated the structural descriptor ζ introduced by Russo and Tanaka[62], also presented in Figure 6. The structural descriptor ζ is defined as the difference between the distance of the closest neighbor molecule which is not hydrogen-bonded to a specific water molecule and the distance of the furthest neighbor molecule which is hydrogen-bonded to the same water molecule. As it can be clearly seen, in the region where q, q_3 and S_q exhibit their local extrema, ζ changes its sign from positive to negative values. The negative value of ζ results from the inter-penetration of the short-range local HB network of the individual water molecules by non-hydrogen-bonded neighbors. As long as ζ is positive, this inter-penetration does not take place. Therefore q and q_3 become more enhanced as the density

increases, reaching their maximum values at the density range where ζ becomes zero. When ζ becomes negative, a local orientational disorder is induced due to the inter-penetration of the local HB network, causing the decrease of q and q_3 at higher densities and the increase of S_q. All these findings clearly indicate the existence of a structural transition in the density region around 3.4 ρ_c and T=1.03 T_c in SCW. Interestingly, Trachenko and coworkers have estimated the location of the Frenkel line, characterizing structural transitions from a "non-rigid" liquid-like fluid to a "rigid" liquid, for temperatures close to 1.03 T_c at a very similar density range[19] (see Figure 2b of Ref. 19). In their approach, they have used the changes in the shape of the molecular velocity autocorrelation function, more specifically the disappearance of its first minimum at short-time scales, as a criterion to identify the boundaries for this structural transition. Our approach, based upon the investigation of orientational and translational order parameters and corresponding entropic quantities, reveals the existence of this kind of structural transitions from a different point of view.

3.2. Thermodynamic Properties.

The density dependence of the calculated pressure is presented in Figure 7, in comparison with available experimental data up to pressures of about 1 GPa, from the databases of the National Institute of Standards and Technology (NIST) and references therein[63,64]. In the density range 0.05 - 2.0 ρ_c the pressure-density curve (inset figure) exhibits a sigmoidal shape, with an almost plateau-like behavior in the range 0.4-1.2 ρ_c and an inflection point around 0.8 ρ_c, where the local density inhomogeneities are more pronounced. On the other hand, the shape of the pressure-density curve is very different in the range 2.2 - 4.6 ρ_c, with the derivative $dP/d\rho_r$, where $\rho_r = \rho/\rho_c$, increasing more rapidly at densities higher than 3.4 ρ_c. Using the calculated values of the pressure corresponding to each one of the investigated densities, extensive NPT Monte Carlo (MC) simulations were subsequently performed in order to calculate the constant pressure specific heat C_p. The constant pressure specific heat C_p has been calculated from the configurational enthalpy H_{conf} ($H_{conf} = U^{pot} + P \cdot V$) fluctuations of the system:

$$C_p = \frac{1}{NRT^2}\left(\left\langle {H_{conf}}^2 \right\rangle - \left\langle H_{conf} \right\rangle^2\right) + 3R \quad (5)$$

In the case of MC simulations, the constant 3R is added to account for the classical kinetic energy contributions from the translation and rotation of the water molecules, as pointed out previously[65,66].

The pressure dependence of C_p is also presented in Figure 7. The corresponding error bars in the calculation of C_p are in the range of about 5 % and certainly do not affect the trends observed in Figure 7. In the pressure range 0.12 – 5.7 GPa a crossover is observed around 1.17 GPa, which corresponds to a density of 3.4 ρ_c. This crossover can be more clearly observed when plotting the pressure dependence of the derivative dC_p / dP, presented as an inset picture in Figure 7. From this inset picture it can be observed that the decay of C_p in the pressure range 0.12-1.17 GPa, corresponding to the 2.2-3.4 ρ_c density range, is very steep and this is also reflected on the non-zero, negative dC_p / dP derivative values. However, at higher pressures in the range 1.17-5.7 GPa (and corresponding density range 3.4-4.6 ρ_c) C_p remains almost constant. In this particular pressure and density range (1.17-5.7 GPa, 3.4-4.6 ρ_c), the derivative dC_p / dP exhibits a constant, nearly zero value. This is a clear indication of this crossover, which is more clearly reflected on the dC_p / dP derivative. This particular behavior of the pressure and the isobaric specific heat further indicate the existence of the structural transitions in SCW around 3.4 ρ_c. On the other hand, in the range 0.2-2.0 ρ_c, the specific heat C_p is maximized around 0.8 ρ_c. This behavior is depicted in the third inset plot of Figure 7, representing the density dependence of C_p at the density range 0.2-2.0 ρ_c. As pointed out earlier, the location of the maxima of C_p has been used to identify the crossing of the Widom line. Interestingly, C_p and the local density augmentation are maximized in the same density range[13,15,39]. Such a finding indicates that the existence of the Widom line and the corresponding structural transition in SCW is closely related to the local density augmentation.

As mentioned in section 2.2, the conversion of liquid-like SCW to a fcc plastic crystal polymorph is observed at 8.5 GPa. This conversion corresponds to a first-order phase transition, which is further verified by the discontinuous change in the density of the system at 8.5 GPa depicted in Figure 8, where the calculated density-pressure diagram corresponding to the pressure range 2-11 GPa is presented. This melting transition, characterized by a first-order singularity, can therefore be distinguished from structural transitions such as the Widom and Frenkel lines. The latter ones, as mentioned in our previous works[39], are characterized by maxima or crossovers in thermodynamic quantities and during these transitions significant but not abrupt changes of thermophysical properties can be observed.

3.3. Dynamic-Transport Properties.

The dynamics of the short-range local structural network around the water molecules were investigated by calculating the density dependence of the intermittent HB lifetime, presented in Figure 9. A crossover at densities around 3.4 ρ_c is observed and can be considered as another indication of the structural transition taking place around 3.4 ρ_c. The molecular reorientational dynamics was also studied in terms of the Legendre reorientational correlation time correlation functions for the O-H intramolecular vectors of the water molecules. A Legendre reorientational time correlation function $C_{\ell R}(t)$ for a specific intramolecular vector and its corresponding correlation time $\tau_{\ell R}$ are defined as:

$$C_{\ell R}(t) = P_{\ell}\left\langle \vec{u}_i(0)\cdot\vec{u}_i(t)\right\rangle \quad , \quad \tau_{\ell R} = \int_0^{\infty} C_{\ell R}(t)\cdot dt \tag{6}$$

In Eq. 6 $\vec{u}_i$ is a unit intramolecular vector associated with a molecule *i*, and P_{ℓ} is a Legendre polynomial of order ℓ. The density dependence of the calculated average first order Legendre reorientational correlation time τ_{1R} for the O–H unit intramolecular vectors of water molecules, is also presented in Figure 9. We may see that the shape of the curve changes at 3.4 ρ_c, exhibiting an inflection point at this particular density. This finding also indicates the effect of the above-mentioned structural transition around 3.4 ρ_c on water

reorientational dynamics. The intermittent dynamics of the hydrogen bonds formed between the water molecules have also been investigated in terms of the HB time-correlation functions $C_{HB}(t)$ and their corresponding HB lifetime τ_{HB}:

$$C_{HB}(t) = \frac{\left\langle h_{ij}(0) \cdot h_{ij}(t) \right\rangle_{t^*}}{\left\langle h_{ij}(0)^2 \right\rangle} \quad , \; \tau_{HB} = \int_0^\infty C_{HB}(t) \cdot dt \tag{7}$$

The variable h_{ij} is such as $h_{ij}(t) = 1$ when a hydrogen bond between specific atoms of the molecules i, j is formed at times 0 and t, and the same hydrogen bond has not been broken for a period longer than t^*, otherwise, $h_{ij}(t) = 0$. The limiting cases, with $t^* = 0$ and $t^* = \infty$, describe the continuous and intermittent dynamics, respectively. When $t^* = 0$ the dynamics corresponds to the continuous one, where no bond breakings and consequent reformations in the time interval [0, t] are observed. When $t^* = \infty$ the dynamics corresponds to the intermittent one. In this case, the persistence probability at time t of a hydrogen bond created at t=0 is investigated, regardless of multiple breakings and reformations of this bond during the time interval [0, t]. The calculated intermittent HB lifetimes $\tau_{HB}{}^{I}$ are presented in Figure 9. A crossover at densities around 3.4 ρ_c is observed in this figure and can be considered as another indication of the above-mentioned structural transition.

The density dependence of the translational self-diffusion coefficient of water, calculated using the well-known Einstein relation, in the range 2.2 - 4.6 ρ_c is also presented in Figure 9. Note that at comparable thermodynamic conditions (T=1.04 T_c, ρ=2.17 ρ_c) the experimentally measured value[67] for the self-diffusion coefficient of SCW is $47.4 \cdot 10^{-9} m^2 / s$, which is in good agreement with the calculated value of $43.16 \cdot 10^{-9} m^2 / s$ at T=1.03 T_c and ρ=2.2 ρ_c. The experimental self-diffusion coefficients of SCW at T=1.01 T_c and in the density range 2.2-2.8 ρ_c [68] (Figure 3 of Reference 68) are also in agreement with the calculated values presented herein at T=1.03 T_c and the same density range, further validating the accuracy of the SPC/E model. From Figure 9 it can be seen that D decreases across this particular density range by about one order of magnitude. On the other hand, the reorientational correlation time of the O-H vector increases only by a factor

of about 1.5. Interestingly, although at 4.6 ρ_c the calculated self-diffusion coefficient of SCW is only about 1.7 times higher than the corresponding value for ambient liquid water calculated with the same potential model[69], the corresponding reorientational correlation time τ_{1R} for the O–H vector is about 18 times lower than the value obtained by the SPC/E model[70] at ambient conditions. These findings clearly indicate that the translational motions of the water molecules are much more strongly affected by the pressure and density increase than the rotational ones, with the latter being significantly faster. SCW at high densities and pressure resembles a liquid-like system where rotation is much more pronounced over the significantly hindered translation, a picture in agreement with the concept of a "rigid" liquid.

In order to provide a quantitative description of the balance between rotational and translational motions in SCW in respect to the ambient liquid, we introduced a coupling parameter $\alpha^{rot/trans}$:

$$\alpha^{rot/trans} = \frac{(\tau_{1R}{}^{amb} / \tau_{1R}{}^{SCW})}{(D^{SCW} / D^{amb})} \quad (8)$$

D^{amb} and $\tau_{1R}{}^{amb}$ are the calculated self-diffusion coefficient and the first-order Legendre reorientational correlation time of a specific intramolecular vector (in this case the O-H vector) of ambient liquid water[69,70]. Note that the fraction $\tau_{1R}{}^{amb} / \tau_{1R}{}^{SCW}$ has been used since $\tau_{\ell R}$, where ℓ is the order of the Legendre polynomial, is inversely proportional to the rotational diffusion[70]. The density dependence of $\alpha^{rot/trans}$ in the density range 2.2-4.6 ρ_c, presented in Figure 9 as an inset figure , exhibits a crossover in the density range around 3.6 ρ_c. This finding is consistent with the hypothesis of the structural transition from a "non-rigid" liquid-like fluid to a "rigid" liquid and can be considered as an additional indication of the existence of this structural transition.

3.4. Plastic crystal phase of SCW at extreme pressures.

The observation of plastic crystal polymorphs of water at subcritical temperatures and elevated pressures has been reported only in classical[29-32,36,37] and reactive force-field[33] simulation studies so far. Some evidence of the existence of the plastic crystal phase at the

600-800 K temperature range has also been reported in classical[29,35] and *ab initio* molecular simulation studies[34]. However, a detailed analysis of the structure and dynamics of these plastic crystal phases, as well as the transformation boundaries and mechanisms between the so-far computationally reported polymorphs, at supercritical conditions is still missing.

From the experimental point of view, previous studies[71] revealed a first order phase transition from liquid water to a solid phase at 400 K and pressures above 7 GPa. The existence of a new crystal phase in the pressure range from 20 to 42 GPa and a wide temperature range has also been reported experimentally[72]. However, the structure of these phases could not be identified in these experiments and the experimental verification still appears to be very challenging.

In this particular study we observed the existence of a face-centered-cubic (fcc) plastic crystal phase of water at pressures higher than 8.5 GPa along the1.03 T_c isotherm, verified by the shape of the calculated O-O and O-H rdf presented in Figure 10. The reorientational dynamics of the O-H vector of the water molecules was also investigated in terms of the first order Legendre reorientational time correlation function $C_{1R}(t)$, which is presented in Figure 10 together with the one corresponding to the liquid-like SCW at 4.6 ρ_c. From this figure it can be clearly seen that the decay of $C_{1R}(t)$ corresponding to the fcc plastic crystal phase at 5.178 ρ_c is faster in comparison with the one corresponding to the liquid-like SCW at 4.6 ρ_c, indicating that the rotation of the water molecules in the fcc plastic crystal is faster in comparison with the liquid-like phase of SCW, although the liquid-like phase is observed at lower densities.

The calculated oxygen atomic velocity time correlation functions $C_v^O(t)$ and their spectral densities $S_v^O(\omega)$ (in the inset picture) of the simulated fcc plastic crystal polymorph at 5.178 ρ_c and the liquid-like SCW at 4.6 ρ_c are also presented in Figure 10. From this figure it can be observed that the low-frequency translational modes in the fcc plastic crystal phase of SCW due to the intermolecular interactions and corresponding cage effects, causing vibrations around the plastic crystal lattice sites, are significantly hindered. This behavior is clearly reflected on both the short-time decay of $C_v^O(t)$, with a more pronounced negative part at very short time-scales, as well as on the blueshift of the low-

frequency peak of $S_v^O(\omega)$ from 122 to 175 cm^{-1} when going from the liquid-like SCW to the fcc plastic crystal phase, respectively.

4. Conclusions

In the present treatment a systematic investigation of the thermodynamic, structural and dynamic properties of SCW has revealed that a near-critical isotherm (T=1.03 T_c) can be divided in several different domains, where water exhibits a very distinct behavior.

By calculating a wide variety of structural order parameters, thermodynamic and dynamic properties of SCW we provide solid evidence about the existence of a structural transition from a "non-rigid" liquid-like fluid to a "rigid" liquid in the density and pressure region around 3.4 ρ_c and 1.17 GPa, respectively, at the near-critical isotherm with T=1.03 T_c. Our approach directly attributes the introduction of the Frenkel line in the literature to the above-mentioned structural transitions in high-density SCW, using a wide variety of structural, thermodynamic and dynamic property descriptors. More specifically, we revealed that in the density range 2.0- 3.4 ρ_c water resembles a more homogeneous "non-rigid" liquid-like fluid, while at densities higher than 3.4 ρ_c it becomes a long-range ordered, tightly packed "rigid" liquid. At densities around 5.2 ρ_c water converts to a plastic crystal polymorph where the molecules rotate faster than in the tightly packed "rigid" liquid-like phase.

Our findings are also correlated to the results of previous studies in the density range 0.05-2.0 ρ_c. These previous studies[39,73], focusing on the volume expansion of the solvation shell containing the four closest water neighbors at low densities and the fluctuations of the interaction energy within the first solvation shell of water, revealed the existence of a crossover at the density range around 0.2 ρ_c. That crossover had been attributed to a structural transition from a supercritical fluid to a gas-like system where the water molecules tend to locate randomly around a central molecule. At densities lower than 0.2 ρ_c SCW resembles a dilute gas consisted of randomly distributed molecules.

On the other hand, our study revealed that the Widom line is located around 0.8 ρ_c . Interestingly, the local density augmentation is maximized in the same density range[13,15,39]. Therefore, the structural crossover associated to the Widom line is distinct from the above-

mentioned transition at 0.2 ρ_c. Taking into account that the Widom line is considered as the boundary between a gas-like and a liquid-like fluid[39,74], we may say that in the density range 0.2 - 0.8 ρ_c near-critical SCW consists of small isolated clusters interacting like gas-phase molecules inside a vacuum environment. However, in the range 0.8-2.0 ρ_c SCW could be described as a continuous condensed medium consisting of voids and clusters of different density, resembling an inhomogeneous porous liquid-like fluid.

The pressure-induced structural transitions along the investigated near-critical isotherm of SCW are schematically represented in Figure 11, providing an overall description of these phenomena taking place close to the critical point of water. The findings of the present study may serve as a springboard for breakthrough future experimental work to further investigate these phenomena in SCW, as well as in other supercritical fluids.

Acknowledgements

The use of the computational facilities of the Computer Simulation in Condensed Matter Research Group (SIMCON) at the Physics Department of the Technical University of Catalonia (UPC) and of the Physical Chemistry Laboratory at the Chemistry Department of the National and Kapodistrian University of Athens (NKUA) is gratefully acknowledged. E. G. acknowledges financial support from the Ministerio de Ciencia, Innovación y Universidades of Spain, Grant PGC2018-099277-B-C21 (MCIU/AEI/ERDF).

References

1) Stanley, H.E. *Introduction to Phase Transitions and Critical Phenomena*, Oxford University Press, 1971.

2) Atkins, P.; de Paula, J. *Physical Chemistry Eighth Edition*, W.H. Freeman and Company, New York, 2006.

3) Tucker, S.C. Solvent Density Inhomogeneities in Supercritical Fluids. *Chem. Rev.* **1999**, *99*, 391-418.

4) Simeoni, G.G.; Bryk, T.; Gorelli, F.A.; Krisch, M.; Ruocco, G.; Santoro, M.; Scopigno, T. The Widom line as the crossover between liquid-like and gas-like behaviour in supercritical fluids. *Nat. Phys.* **2010**, *6*, 503-507.

5) McMillan, P. F.; Stanley, H.E. Going supercritical. *Nat. Phys.* **2010**, *6*, 479-480.

6) Brazhkin, V.V., Fomin, Y.D.; Lyapin, A.G.; Ryzhov, V.N.; Tsiok, E.N. Widom line for the liquid-gas transition in Lennard-Jones system. *J. Phys. Chem. B* **2011**, *115*, 14112-14115.

7) Gorelli, F.A.; Bryk, T.; Krisch, M.; Ruocco, G.; Santoro, M.; Scopigno, T. Dynamics and Thermodynamics beyond the critical point. *Sci. Rep.* **2013**, *3*, 1203.

8) Gallo, P.; Corradini, D.; Rovere, M. Widom line and dynamical crossovers as routes to understand supercritical water. *Nat. Commun.* **2014**, ***5***, 586.

9) Maxim, F.; Contescu, C.; Boillat, P.; Niceno, B.; Karalis, K.; Testino, A. Visualization of supercritical water pseudo-boiling at Widom line crossover. *Nat. Commun.* **2019**, *10*, 4114.

10) Karalis, K.; Ludwig, C.; Niceno, B. Supercritical water anomalies in the vicinity of the Widom line. *Sci. Rep.* **2019**, *9*, 15731.

11) Ha, M.Y.; Yoon, T. J.; Tlusty, T.; Jho, Y.; Lee, W. B. Widom Delta of Supercritical Gas–Liquid Coexistence. *J. Phys. Chem. Lett.* **2018**, *9*, 1734-1738.

12) Schienbein, P.; Marx, D. Investigation concerning the uniqueness of separatrix lines separating liquidlike from gaslike regimes deep in the supercritical phase of water with a focus on Widom line concepts. *Phys. Rev. E* **2018**, *98*, 022104.

13) Skarmoutsos, I.; Dellis, D.; Samios, J. The effect of intermolecular interactions on local density inhomogeneities and related dynamics in pure supercritical fluids. A comparative molecular dynamics simulation study. *J. Phys. Chem. B* **2009**, *113*, 2783-2793.

14) Skarmoutsos, I.; Samios, J. Local density augmentation and dynamic properties of hydrogen-and non-hydrogen-bonded supercritical fluids: A molecular dynamics study. *J. Chem. Phys.* **2007**, *126*, 044503.

15) Skarmoutsos, I.; Samios, J. Local Density Inhomogeneities and Dynamics in Supercritical Water: A Molecular Dynamics Simulation Approach. *J. Phys. Chem. B* **2006**, *110*, 21931-21937.

16) Brazhkin, V.V.; Fomin, Yu. D.; Lyapin, A.G.; Ryzhov, V.N.; Trachenko, K. Two liquid states of matter: A dynamic line on a phase diagram. *Phys. Rev. E* **2012**, *85*, 031203.

17) Bolmatov, D.; Brazhkin, V.V.; Trachenko, K. Thermodynamic behaviour of supercritical matter. *Nat. Commun.* **2013**, *4*, 2331.

18) Brazhkin, V.V.; Fomin, Yu. D.; Lyapin, A.G.; Ryzhov, V.N.; Tsiok, E.N.; Trachenko, K. "Liquid-Gas" Transition in the Supercritical Region: Fundamental Changes in the Particle Dynamics. *Phys. Rev. Lett.* **2013**, *111*, 145901.

19) Yang, C.; Brazhkin, V.V.; Dove, M.T.; Trachenko, K. Frenkel line and solubility maximum in supercritical fluids. *Phys. Rev. E* **2015**, *91*, 012112.

20) Fomin, Yu. D.; Ryzhov, V. N.; Tsiok, E. N.; Brazhkin, V.V. Dynamical crossover line in supercritical water. *Sci. Rep.* **2015**, *5*, 14234.

21) Bolmatov, D.; Zhernenkov, M.; Zav'yalov, D.; Tkachev, S. N.; Cunsolo, A.; Cai, Y. Q. The Frenkel Line: A Direct Experimental Evidence for the New Thermodynamic Boundary. *Sci. Rep.* **2015**, *5*, 15850 (2015).

22) Cockrell, C.; Dicks, O.A.; Brazhkin, V.V.; Trachenko, K. Pronounced structural crossover in water at supercritical pressures. *J. Phys.: Condens. Matter* **2020**, *32*, 385102.

23) Bryk, T.; Gorelli, F.A.; Mryglod, I.; Ruocco, G.; Santoro, M.; Scopigno, T. Behavior of Supercritical Fluids across the "Frenkel Line". *J. Phys. Chem. Lett.* **2017**, *8*, 4995-5001.

24) Brazhkin, V.V.; Prescher, C.; Fomin, Yu. D.; Tsiok, E. N.; Lyapin, A. G.; Ryzhov, V. N.; Prakapenka, V.B.; Stefanski, J.; Trachenko, K.; Sapelkin, A. Comment on "Behavior of Supercritical Fluids across the 'Frenkel Line'. *J. Phys. Chem. B* **2018**, *122*, 6124–6128.

25) Bryk, T.; Gorelli, F.A.; Mryglod, I.; Ruocco, G.; Santoro, M.; Scopigno, T. Reply to "Comment on 'Behavior of Supercritical Fluids across the Frenkel Line'. *J. Phys. Chem. B* **2018**, *122*, 6120-6123.

26) Weingärtner, H.; Franck, E.U. Supercritical water as a solvent. *Angew. Chem. Int. Ed.* **2005**, *44*, 2672-2692.

27) Galli, G.; Pan, D. A closer look at supercritical water. *Proc. Natl. Acad. Sci. U.S.A.* **2013**, *110*, 6250-6251.

28) Akiya, N.; Savage, Ph. Roles of water for chemical reactions in high-temperature water. *Chem. Rev.* **2002**, *102*, 2725-2750.

29) Aragones, J. L.; Vega, C. Plastic crystal phases of simple water models. *J. Chem. Phys.* **2009**, *130*, 244504.

30) Takii, Y.; Koga, K.; Tanaka, H. A plastic phase of water from computer simulation. *J. Chem. Phys.* **2008**, *128*, 204501.

31) Aragones, J.L.; Conde, M.M.; Noya, E.G.; Vega, C. The phase diagram of water at high pressures as obtained by computer simulations of the TIP4P/2005 model: the appearance of a plastic crystal phase. *Phys. Chem. Chem. Phys.* **2009**, *11*, 543-555.

32) Brukhno, A.V.; Grant, J.; Underwood, T.L.; Stratford, K.; Parker, S.C.; Purton, J.A.; Wilding, N.B. DL_MONTE: a multipurpose code for Monte Carlo simulation. *Mol. Simulat.* **2021**, *47*, 131-151.

33) Adachi, Y.; Koga, K. Structure and phase behavior of high-density ice from molecular-dynamics simulations with the ReaxFF potential. *J. Chem. Phys.* **2020**, *153*, 114501.

34) Hernandez, J.-A.; Caracas, R. Proton dynamics and the phase diagram of dense water ice. *J. Chem. Phys.* **2018**, *148*, 214501.

35) Yoon, J.T.; Patel, L.A; Ju, T.; Vigil, M.J.; Findikoglu, A.T.; Currier, R.P.; Maerzke, K.A. Thermodynamics, dynamics, and structure of supercritical water at extreme conditions. *Phys. Chem. Chem. Phys.* **2020**, *22*, 16051-16062.

36) Henao, A.; Salazar-Rios, J.M.; Guardia, E.; Pardo, L.C. Structure and dynamics of water plastic crystals from computer simulations. *J. Chem. Phys.* **2021**, *154*, 104501.

37) Skarmoutsos, I.; Mossa, S.; Guardia, E. The effect of polymorphism on the structural, dynamic and dielectric properties of plastic crystal water: A molecular dynamics simulation perspective. *J. Chem. Phys.* **2019**, *150*, 124506.

38) Stubbs, J.M. Molecular simulations of supercritical fluid systems. *J. Supercrit. Fluids* **2016**, *108*, 104-122.

39) Skarmoutsos, I.; Guardia, E.; Samios, J. Local structural fluctuations, hydrogen bonding and structural transitions in supercritical water. *J. Supercrit. Fluids* **2017**, *130*, 156-164.

40) Berendsen, H.J.C.; Grigera, J.R.; Straatsma, T.P. The missing term in effective pair potentials. *J. Phys. Chem.* **1987**, *91*, 6269-6271.

41) Guissani, Y.; Guillot, B. A computer simulation study of the liquid-vapor coexistence curve of water. *J. Chem. Phys.* **1993**, *98*, 8221-8235.

42) Alejandre, J.; Tildesley, D.J. Molecular dynamics simulation of the orthobaric densities and surface tension of water. *J. Chem. Phys.* **1994**, *102*, 4574-4583.

43) Guardia, E.; Marti, J. Density and temperature effects on the orientational and dielectric properties of supercritical water. *Phys. Rev. E* **2004**, *69*, 011502.

44) Johansson, E.; Bolton, K.; Ahlström, P. Simulations of vapor water clusters at vapor-liquid equilibrium. *J. Chem. Phys.* **2005**, *123*, 024504.

45) Guardia, E.; Laria, D.; Marti, J. Hydrogen Bond Structure and Dynamics in Aqueous Electrolytes at Ambient and Supercritical Conditions. *J. Phys. Chem. B* **2006**, *110*, 6332-6338.

46) Yoon, J.T.; Patel, L.A; Vigil, M.J.; Maerzke, K.A.; Findikoglu, A.T.; Currier, R.P. Electrical conductivity, ion pairing, and ion self-diffusion in aqueous NaCl solutions at elevated temperatures and pressures. *J. Chem. Phys.* **2019**, *151*, 224504.

47) Dubbeldam, D.; Calero, S.; Ellis, D.E.; Snurr, R.Q. RASPA: molecular simulation software for adsorption and diffusion in flexible nanoporous materials. *Mol. Simulat.* **2016**, *42*, 81-101.

48) Smith, W.; Forester, T.R. DL_POLY_2.0: A general-purpose parallel molecular dynamics simulation package. *J. Mol. Graph.* **1996**, *14*, 136-141.

49) Allen, M. P.; Tildesley, D. J. *Computer Simulations of Liquids*, Oxford University Press, Oxford, 1987.

50) Hoover, W.G. Canonical dynamics: Equilibrium phase-space distributions. *Phys. Rev. A* **1985**, *31*, 1695-1697.

51) Hoover, W.G. Constant-pressure equations of motion. *Phys. Rev. A* **1986**, *34*, 2499-2500.

52) Lin, S.-T.; Blanco, M.; Goddard III, W.A. The two-phase model for calculating thermodynamic properties of liquids from molecular dynamics: Validation for the phase diagram of Lennard-Jones fluids. *J. Chem. Phys.* **2003**, *119*, 11792.

53) Lin, S.-T.; Maiti, P.K.; Goddard III, W.A. Two-Phase Thermodynamic Model for Efficient and Accurate Absolute Entropy of Water from Molecular Dynamics Simulations. *J. Phys. Chem. B* **2010**, *114*, 8191–8198.

54) Caro, M.A.; Laurila, T.; Lopez-Acevedo, O. Accurate schemes for calculation of thermodynamic properties of liquid mixtures from molecular dynamics simulations. *J. Chem. Phys.* **2016**, *145*, 244504.

55) Soper A.K. The radial distribution functions of water and ice from 220 to 673 K and at pressures up to 400 MPa. *Chem. Phys.* **2000**, *258*, 121-137.

56) Skarmoutsos, I.; Guardia, E. Effect of the local hydrogen bonding network on the reorientational and translational dynamics in supercritical water. *J. Chem. Phys.* **2010**, *132*, 074502.

57) Nieto-Draghi, C.; Bonet Avalos, J.; Rousseau, B. Dynamic and structural behavior of different rigid nonpolarizable models of water. *J. Chem. Phys.* **2003**, *118*, 7954-7964.

58) Marti, J. Analysis of the hydrogen bonding and vibrational spectra of supercritical model water by molecular dynamics simulations. *J. Chem. Phys.* **1999**, *110*, 6876-6886.

59) Errington, J.R.; Debenedetti, P. G. Relationship between structural order and the anomalies of liquid water. *Nature* **2001**, *409*, 318–321.

60) Henchman, R.H.; Cockram, S. J. Water's non-tetrahedral side. *Faraday Discuss.* **2013**, 167, 529-550.

61) Kumar, P.; Buldyrev, S.V.; Stanley, H.E. A tetrahedral entropy for water. Proc. Natl. Acad. Sci. U.S.A. **2009**, *106*, 22130-22134.

62) Russo, J.; Tanaka, H. Understanding water's anomalies with locally favoured structures. *Nat. Commun.* **2014**, *5*, 3556.

63) Saul A.; Wagner, W. A Fundamental Equation for Water Covering the Range from the Melting Line to 1273 K at Pressures up to 25 000 MPa. *J. Phys. Chem. Ref. Data* **1989**, *18*, 1537-1564.

64) Wagner, W.; Pruß A. The IAPWS Formulation 1995 for the Thermodynamic Properties of Ordinary Water Substance for General and Scientific Use. *J. Phys. Chem. Ref. Data* **2002**, *31*, 387-535.

65) Kalinichev, A.G. Monte Carlo Simulations of Water under Supercritical Conditions. I. Thermodynamic and Structural Properties. *Z. Naturforsch.* **1991**, *46 a*, 433-444.

66) Teplukhin, A.V. Monte Carlo Calculation of the Thermodynamic Properties of Water. *J. Struct. Chem.* **2013**, *54*, 221-232.

67) Lamb, W.J.; Hoffman, G.A.; Jonas, J. Self-diffusion in compressed supercritical water. *J. Chem. Phys.* **1981**, *74*, 6875-6880.

68) Tassaing, T.; Danten, Y.; Besnard, M. Supercritical water: Local order and molecular dynamics. *Pure Appl. Chem.* **2004**, *76*, 133–139.

69) Tazi, S.; Boţan, A.; Salanne, M.; Marry, V.; Turq, P.; Rotenberg, B. Diffusion coefficient and shear viscosity of rigid water models. *J. Phys.: Condens. Matter* **2012**, *24*, 284117.

70) Laage, D.; Hynes, J.T. On the Molecular Mechanism of Water Reorientation. *J. Phys. Chem. B* **2008**, *112*, 14230-14242.

71) Dolan, D.; Knudson, M.; Hall, C.; Deeney, C. A metastable limit for compressed liquid water. *Nat. Phys.* **2007**, *3*, 339-342.

72) Schwager, B.; Boehler, R. H_2O: another ice phase and its melting curve. *High Press. Res.* **2008**, *28*, 431-433.

73) Ma, H.; Ma, J. Density dependence of hydrogen bonding and the translational-orientational structural order in supercritical water: A molecular dynamics study. *J. Chem. Phys.* **2011**, *135*, 054504.

74) Sedunov, B.I. Structural Transitions in Supercritical Fluids. *Journal of Thermodynamics* **2011**, ID: 194353.

FIGURES

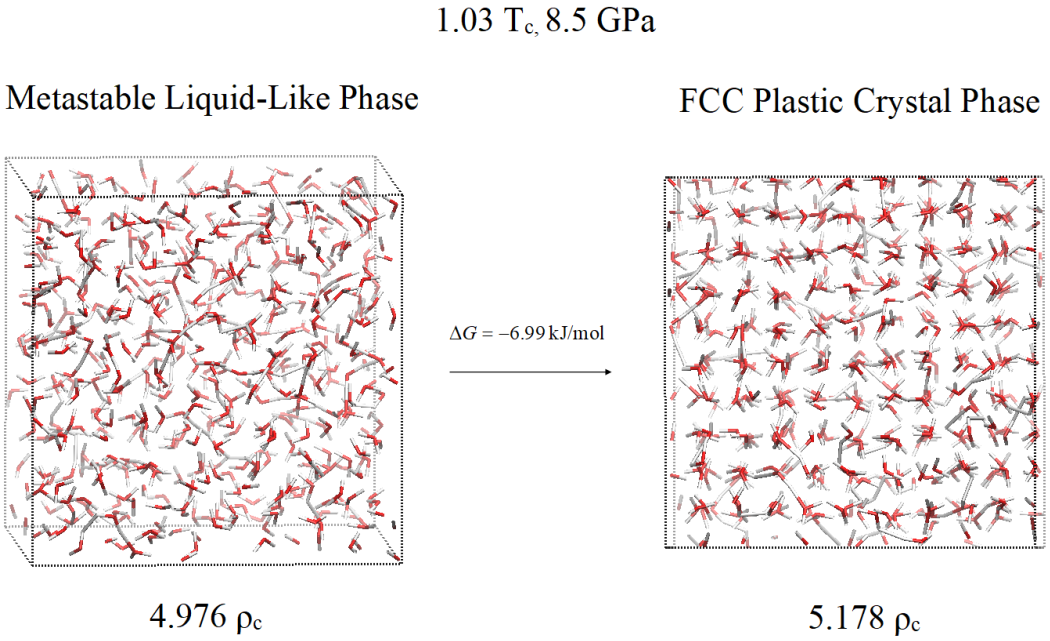

Figure 1: Characteristic snapshots of the simulated metastable, liquid-like phase and the fcc plastic crystal phase of water at T=1.03 T_c and 8.5 GPa.

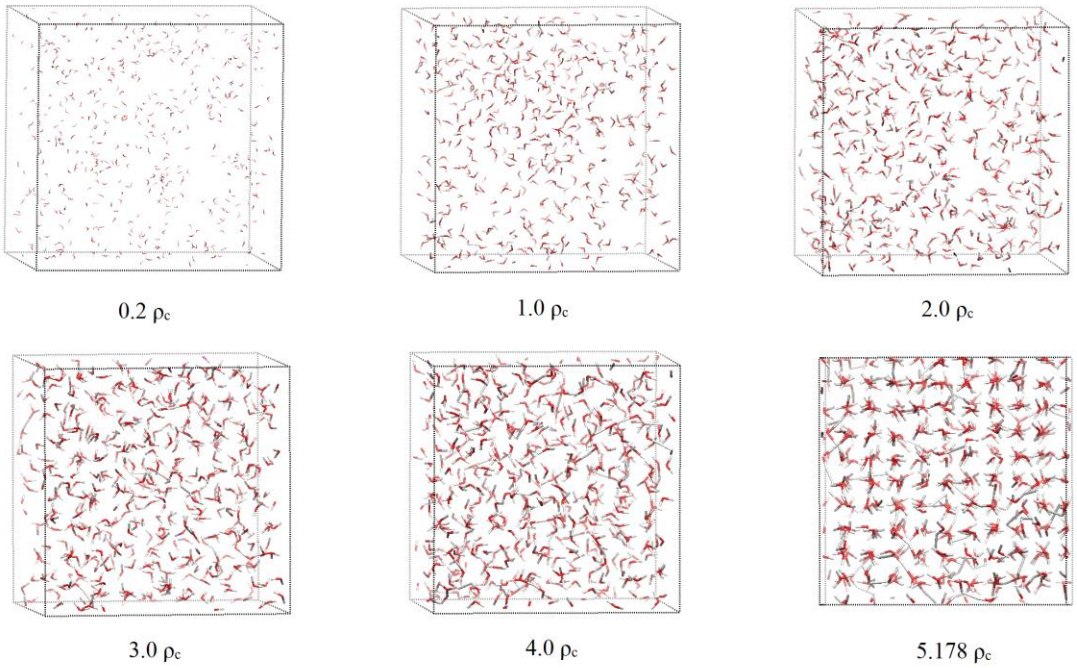

Figure 2: Selective snapshots of the simulated systems, starting from low density SCW (0.2 ρ_c) and going up to the observed fcc plastic crystal phase at 8.5 GPa (5.178 ρ_c).

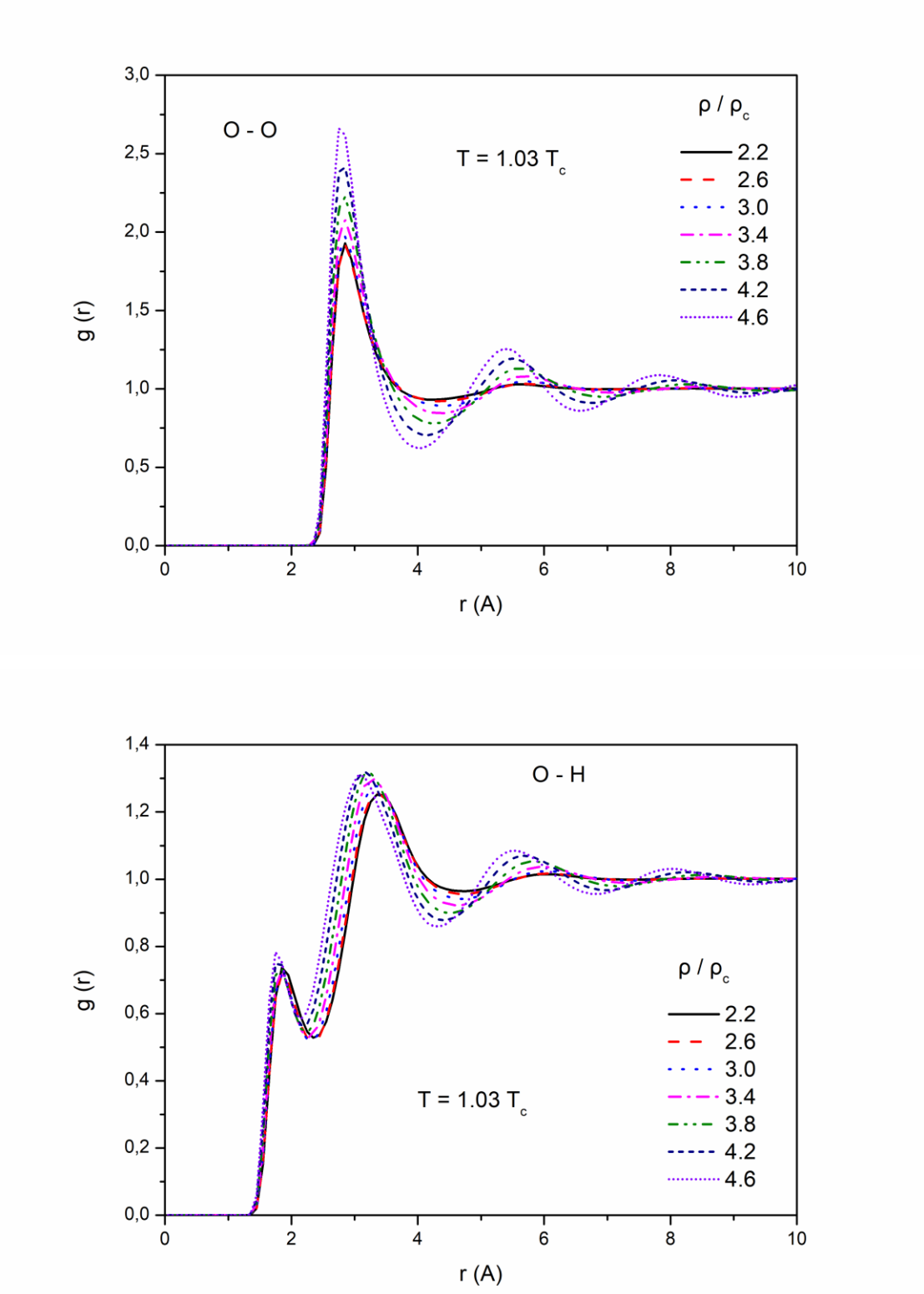

Figure 3: Calculated O-O and O-H pair radial distribution functions at the density range 2.2 - 4.6 ρ_c, along the T=1.03 T_c isotherm.

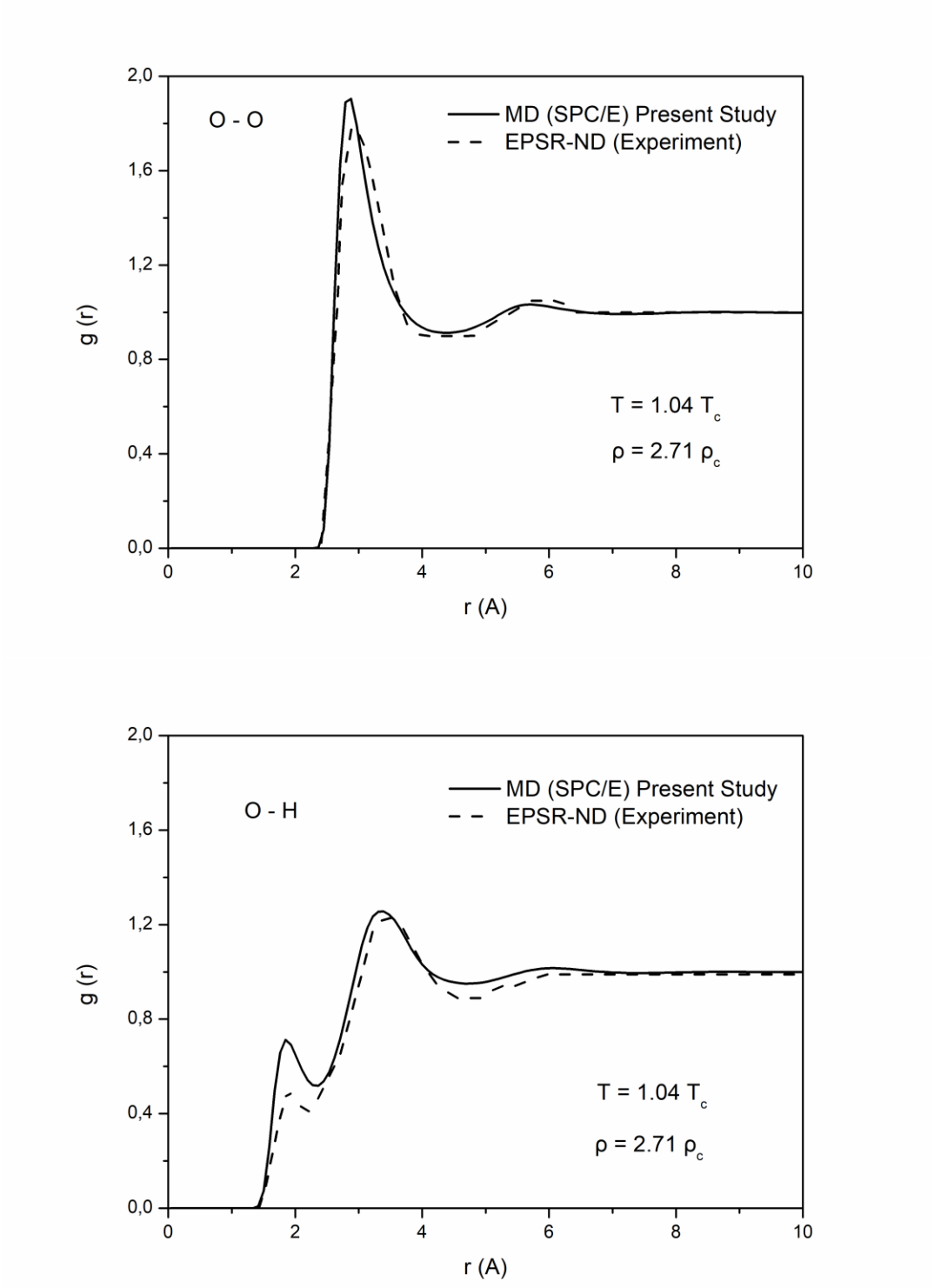

Figure 4: The calculated O-O and O-H pair radial distribution functions at 2.71 ρ_c and T=1.04 T_c (present study), plotted in comparison with the ones obtained by the empirical potential structure refinement of experimental neutron diffraction data[55].

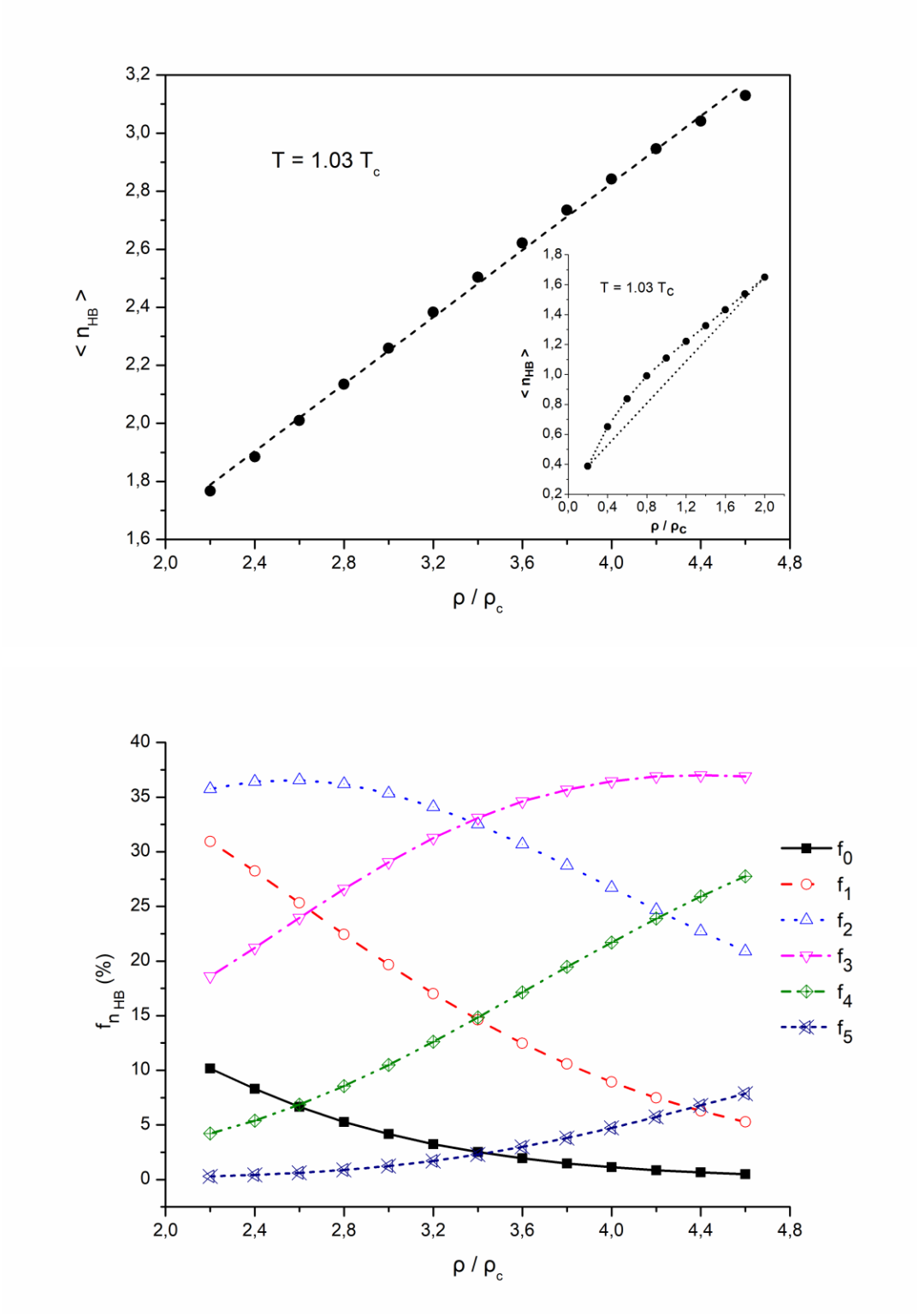

Figure 5: Density dependence of the average number of hydrogen bonds $\langle n_{HB} \rangle$ formed per water molecule and the fraction of water molecules forming 0-5 hydrogen bonds.

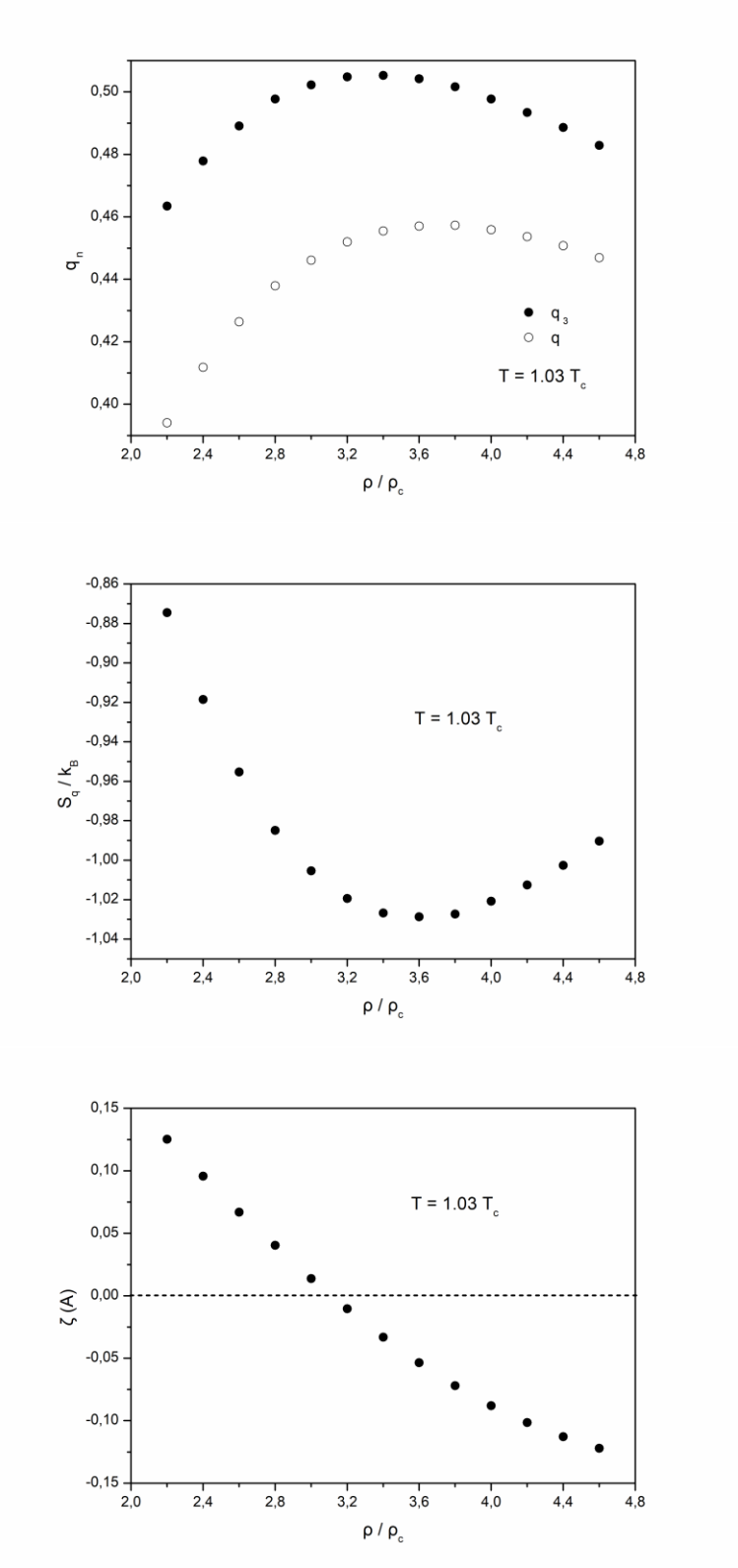

Figure 6: Density dependence of the tetrahedral and trigonal order parameters, the tetrahedral entropy per water molecule and the structural descriptor ζ.

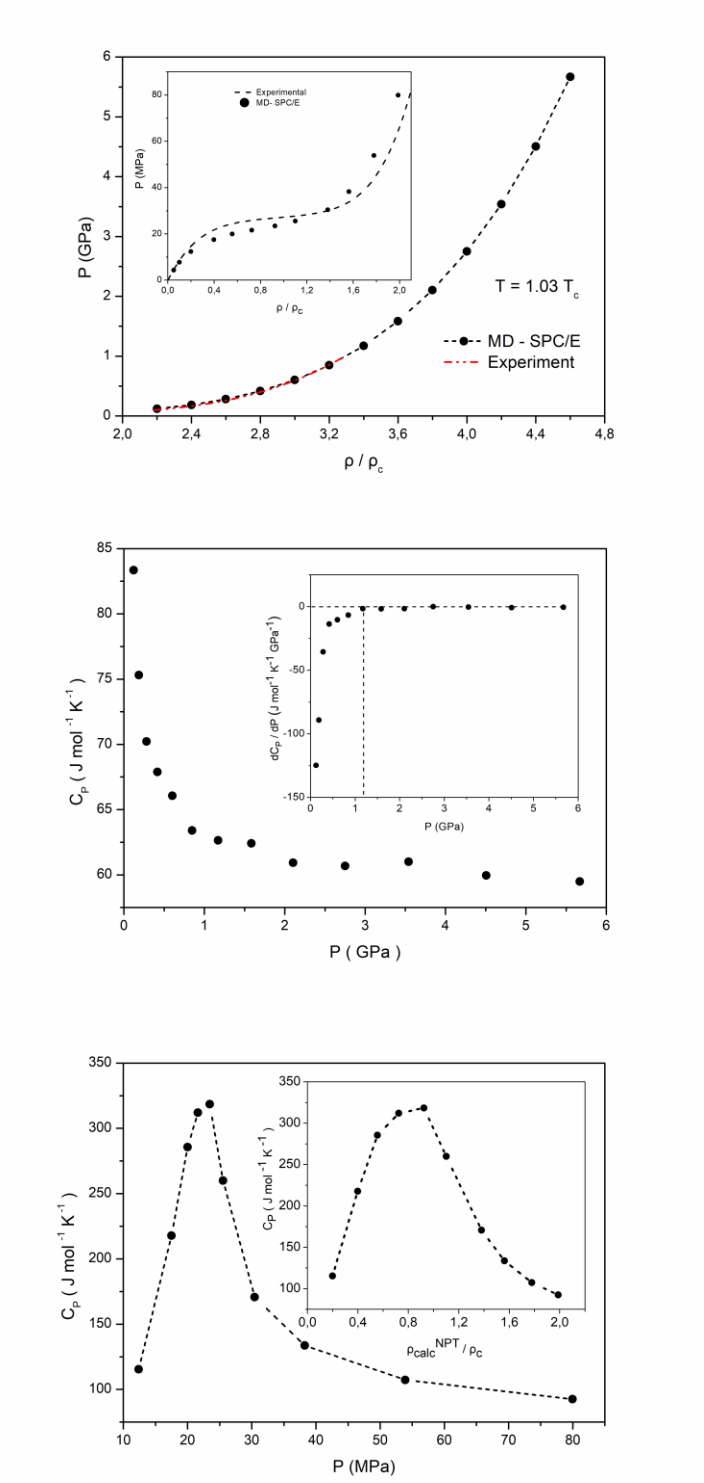

Figure 7: Calculated pressure-density diagrams along the T=1.03 T_c isotherm for the overall density range 0.05 - 4.6 ρ_c and pressure dependence of the calculated specific heat C_p. The pressure dependence of dC_p / dP in the pressure range 0.12-5.7 GPa and the density dependence of C_p in the density range 0.2- 2.0 ρ_c are also presented as inset figures.

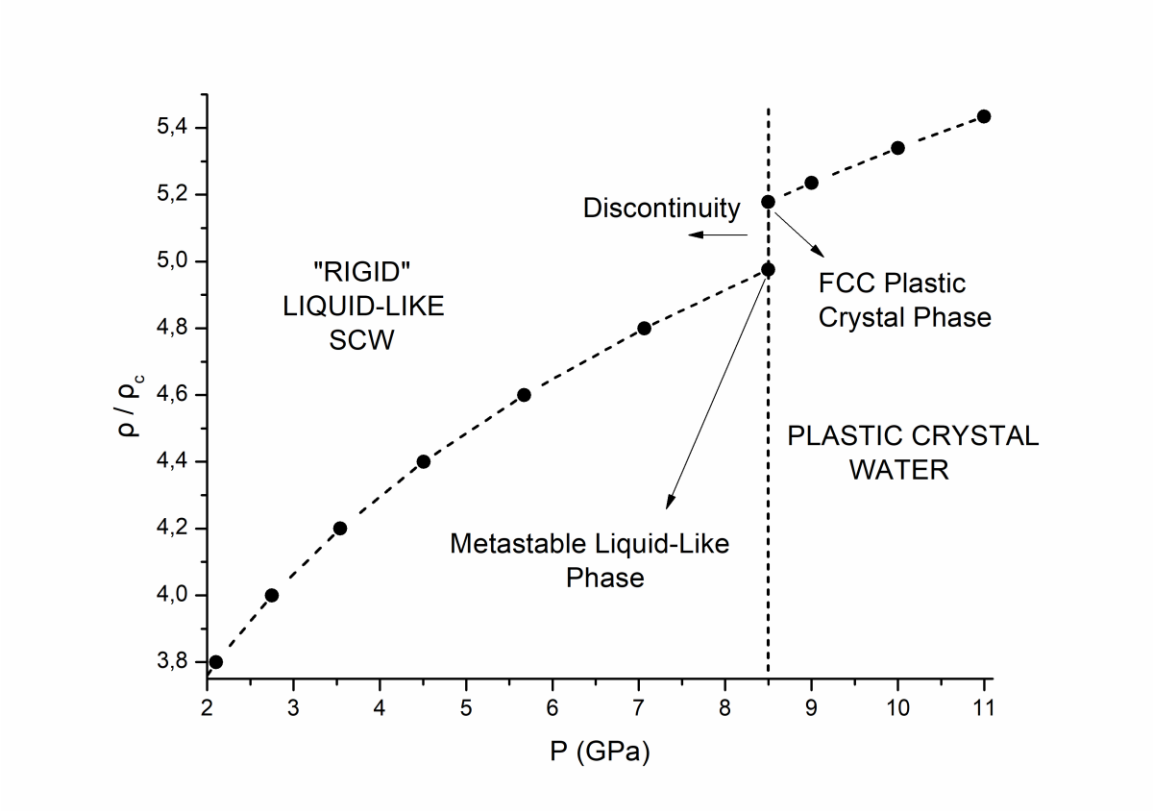

Figure 8: Calculated density-pressure diagram of water at T=1.03 T_c and for the pressure range 2-11 GPa, depicting the discontinuous change in the density when the melting transition takes place.

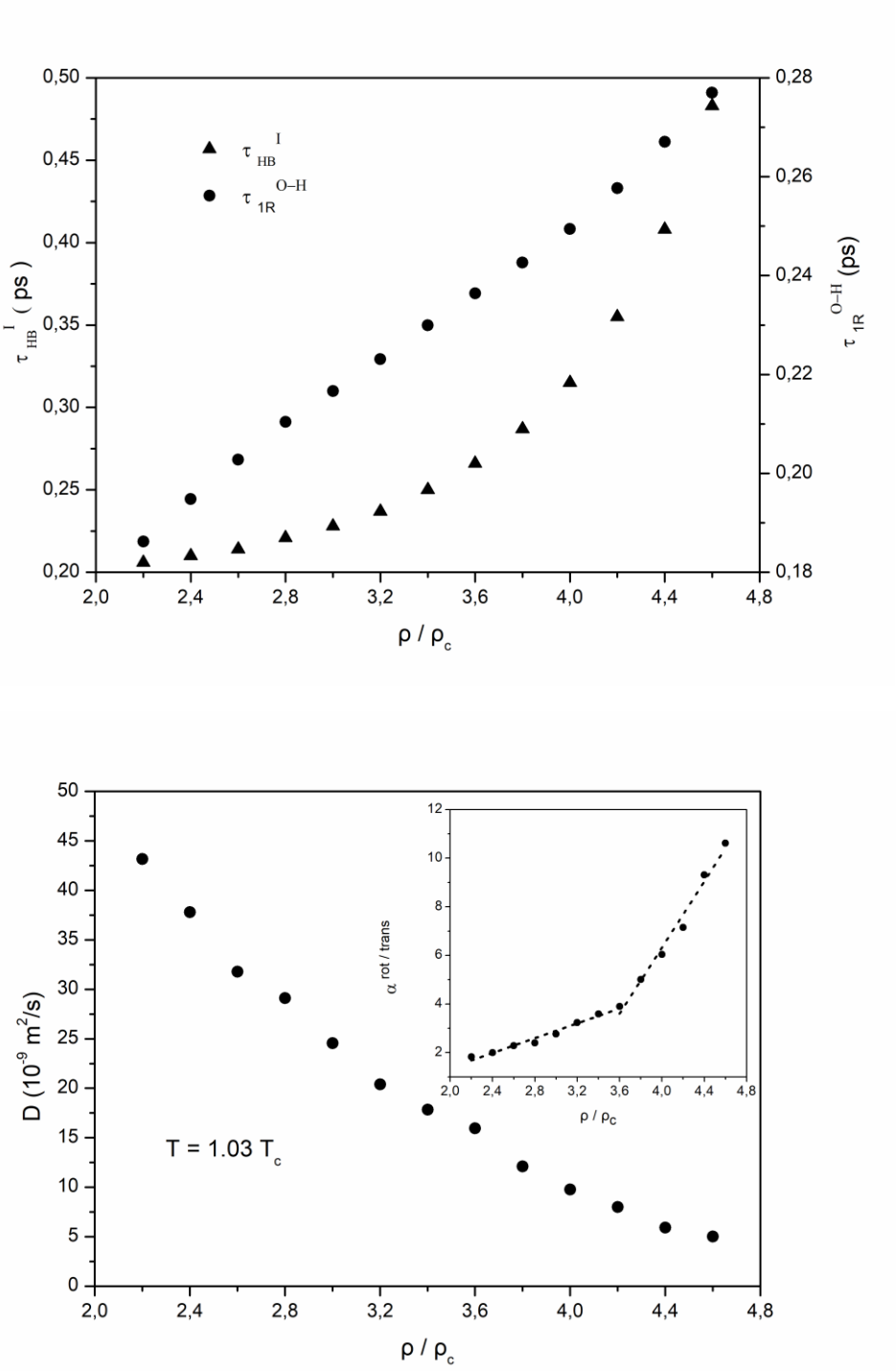

Figure 9: Density dependence of the calculated reorientational correlation time τ_{1R} of the O-H vector of water molecules and HB lifetime $\tau_{HB}{}^{I}$, the self-diffusion coefficient and the coupling parameter $\alpha^{rot/trans}$.

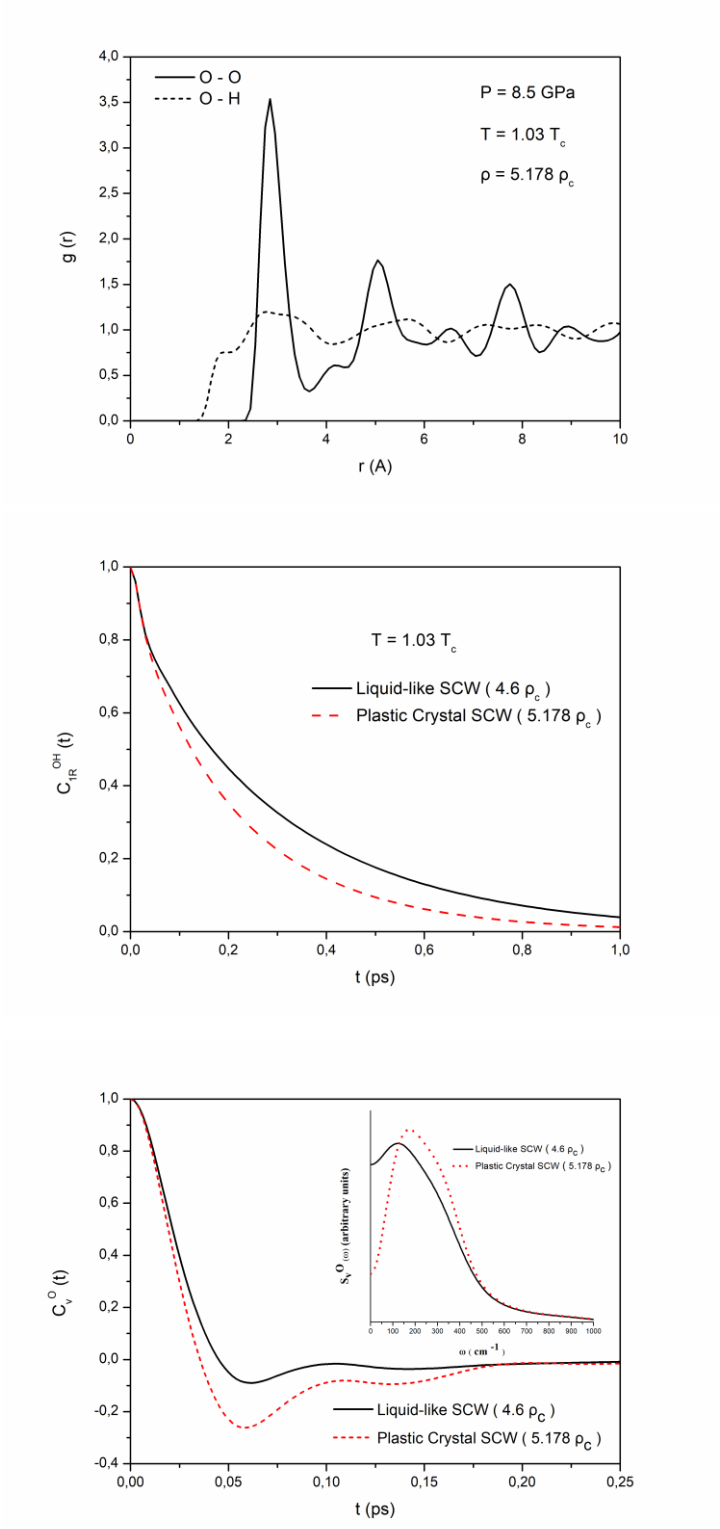

Figure 10: O-O and O-H pair radial distribution functions of the fcc plastic crystal at 5.178 ρ_c, reorientational time correlation functions $C_{1R}(t)$ of the O-H vector and oxygen velocity correlation functions and corresponding spectral densities at 4.6 ρ_c and 5.178 ρ_c.

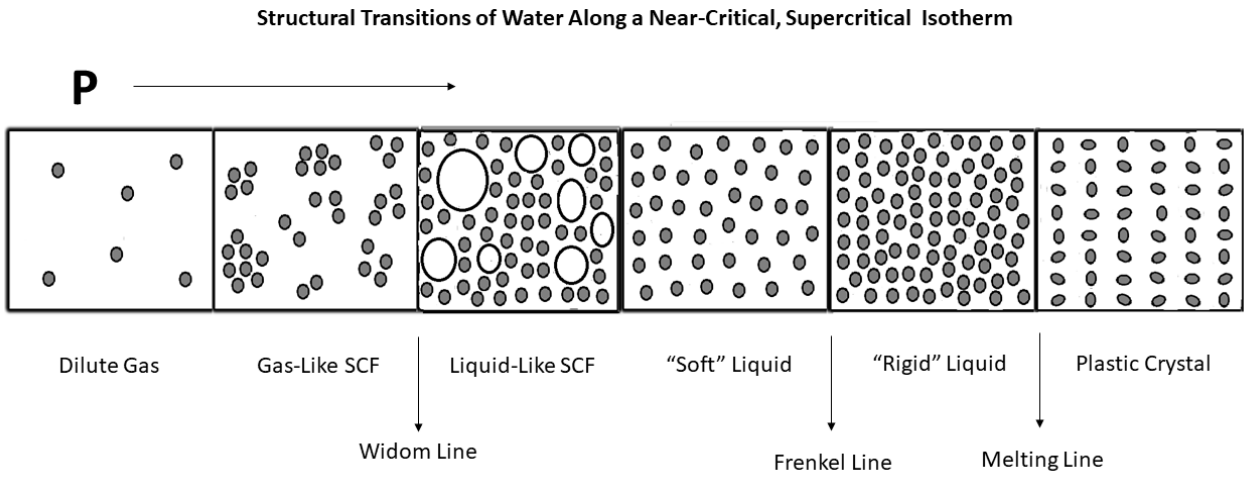

Figure 11: Schematic representation of the observed pressure-induced structural transitions along a near-critical isotherm of SCW.

Table of Contents (TOC) Figure